Engineering Structures 243 (2021) 112409

Contents lists available at ScienceDirect

Engineering Structures

journal homepage: www.elsevier.com/locate/engstruct

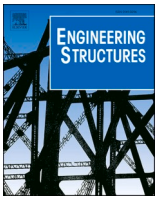

# Lightweight and slender timber-concrete composite floors made of CLT-HPC and CLT-UHPC with ductile notch connectors

Serge Lamothe [a], Luca Sorelli [a,*], Pierre Blanchet [b], Philippe Galimard [c]

[a] Département de Génie Civil, Université Laval, Québec, G1V 0A6, Canada
[b] Department of Wood and Forest Sciences, Université Laval, Québec, G1V 0A6, Canada
[c] Department of Construction Timber Engineering, University of Bordeaux, France

ARTICLE INFO

*Keywords:*
Timber-concrete composite structures
Ductile Notch Connections
Cross Laminated Timber (CLT)
High Performance Concrete (HPC)
Ultra-High Fiber Performance Concrete (UHPFRC)

ABSTRACT

Cross-Laminated Timber (CLT) structures have been emerging worldwide for residential floors in multi-storey buildings thanks to their lightness, fast construction and low ecological footprint. This work aims at fostering this application, which is often limited by vibrational and deflection limits, by investigating composite slab floors made of CLT and High-Performance Concrete (HPC) slab as well as CLT and Ultra High-Performance Fiber Reinforced Concrete (UHPFRC).

Firstly, the composite floors CLT-HPC and CLT-UHPFRC with a span of 8 m were designed by considering a multicriteria analysis. To assure a certain structural ductility, previously developed ductile notch connectors were employed. As an economic choice, no shear reinforcement in the concrete slab was employed. Then, full-scale composite beams were fabricated in order to verify the predicted flexural behaviour and natural frequency. A numerical analysis was carried out to verify the connectors could effectively yield before the timber collapse. The comparison between the numerical simulation and the slip measurements confirmed that about 50% of the notch connections fully yielded and underwent inelastic deformation which favors the structural ductility. In the case of the CLT-HPC floor, a reduction of the notch contact surface due to the use of plastic sheet waterproofing as well as shear cracks developing in the concrete close to the notch corner both reduced the expected structural stiffness. Finally, the CLT-UHPFRC floor is endowed with outstanding values of slenderness ratio (~35) and lightness (~2 kPa), while eliminating the use of shear reinforcement and sheet waterproofing.

## 1. Introduction

In the last decades Cross-Laminated-Timber (CLT) floors have been more and more employed in multistory timber buildings [1–4]. In practise, a concrete slab is often added on top of the timber structure for improving the vibrational behaviour and acoustic insulation [5–6]. By mechanically connecting timber and concrete, Timber-Concrete Composite structures (TCC) allows reducing the thickness, the lightness and the construction time of the floor [7–9]. Moreover, TCC floors can advantageously reduce the environmental imprint especially with respect to traditional concrete floors [10–12].

In TCC structures it is possible to achieve a high degree of composite action by using stiff connectors, such as, steel plates or notches [13–14], which in turn increases the structural stiffness. Moreover, structural ductility is an important consideration as it allows avoiding sudden failures, increasing the energy dissipation, and in the case of continuous beams enhancing the structure reliability, during seismic loadings [15–16]. As timber and concrete have a limited material ductility, TCC structures can be *plastically-designed* by employing ductile connectors as well as assuring a hierarchal sequence of inelastic mechanisms so that the ductile connections efficiently yield before the timber failure [17–19]. Therefore, recent works have developed ductile connections for TCC structures, e.g., perforated steel plates [20], composite elongated connectors [21], and also notch connections [22]. In particular, Selçukoglu and Zwicky developed stiff and ductile notch connection between concrete and Glued Laminated Timber (GLT) by designing the notch configuration so that the wood fibers yield under compression parallel to grain [22]. Following the same principle, by means of push-out tests, Lamothe et al. [23] developed ductile notch connectors for CLT slab and concrete slab by limiting the notch depth for avoiding the rolling shear of timber layer. In particular, a special class of concrete, such as, High-Performance Concrete (HPC) or Ultra-High-Performance

* Corresponding author.
*E-mail address:* luca.sorelli@gci.ulaval.ca (L. Sorelli).

https://doi.org/10.1016/j.engstruct.2021.112409
Received 6 June 2020; Received in revised form 8 January 2021; Accepted 14 April 2021

Fiber Reinforced Concrete (UHPFRC) was employed to reduce the risk of shear crack at the notch corner.

Recently, Jiang and Crocetti [24] tested full-scale CLT-concrete floors with ductile notch connectors with a span of 6.5 m and a remarkable slenderness (i.e., height-to-span ratio) of 35. The rectangular notch connections were reinforced with two lag screws and a vertical stirrup. In spite of the use of ductile notch connections, the structural response was linear and rather brittle. That is, it is possible that the TCC was not plastically designed to allow all connectors to yield before the brittle collapse of the timber slab [22]. Furthermore, TCC floors made of Laminated Veneer Lumber (LVL) timber connected to normal concrete by ductile notch connectors have been developed and tested at full-scale with a span of 5.66 m [25]. In spite of the high slenderness of about 30, the floor lightness was not optimized as the timber height was only 40 mm of the total floor height of 200 mm. Interestingly, their results showed that the addition of shear reinforcement (i.e., stirrups, shear dowels, end-to-end vertical connection, etc.) in the concrete notch can significantly increase the load-carrying capacity, but it does not affect the elastic response of the TCC structure at serviceability load. Finally, Mai et al. developed composite floor made of CLT slab connected with normal concrete slab by screws with a floor slenderness of about 24 [26]. While the natural frequency was satisfactory, the inelastic structural response under static loading strongly depends on the screw spacing and inclination angle.

The use of Ultra-High Performance Fiber Reinforced Concrete (UHPFRC) is particularly appealing for TCC floor [27–29]. Indeed, the high Young's modulus ($E_c \approx$ 50–60 GPa) and compressive strength ($f_c \approx$ 120–180 MPa) of UHPFRC allows designing thin concrete slabs which are ideal lightweight composite floors [30–32]. Furthermore, the low creep of UHPFRC slab allows reducing the long-term deflection of by 50% with respect to an equivalent timber floor [33].

This work aims at fostering TCC floors in terms of slenderness and lightness by connecting a CLT slab to a High-Performance Concrete (HPC) or an UHPFRC slab with ductile notch connections. As main result, an innovative floor solution of exceptional slenderness and lightness without any need of steel shear reinforcement was designed and experimentally validated. To validate the plastically-design approach, a numerical Finite Element model (FEM) for TCC structures was employed. For engineering purpose, the accuracy of existing design methods to predict the structural stiffness and strength of the developed composite floor is also discussed.

## 2. Materials and methods

### 2.1. Existing models for TCC beams

This section briefly presents some existing methods for predicting the structural response of TCC beams. The goal of the modeling part is to assess the applicability of existing analytical models to predict the serviceability deflection limits as well as the ultimate load, which is of practical importance for engineers.

Moreover, we will employ a Finite Element model for TCC structure which is called DDuctileTCS® which has been developed at Université Laval and well-validated on TCC structures [30,34–35] with the goal to assess the amount of connectors which have effectively yielded at collapse, which is at the core of the plastically-designed approach of a ductile TCC structure.

#### 2.1.1. Linear γ-method

The γ-method as adopted in the Annex B of the Eurocode 5 [36] allows predicting the structural stiffness from the connection stiffness. The method is an linear elastic solution for a composite beam with a linear relationship between shear and slip, i.e., $V = K \times s$, where $V$ is the connection force, $K$ is the connection stiffness, $s$ is the slip [37]. The slip modulus is $k = K/e$ where $e$ is the connection spacing. The shear coefficient $\gamma$ is defined as follows:

$$\gamma = \frac{1}{1 + \frac{\pi^2 A_c E_c}{kL^2}} \tag{1}$$

where $E_c$ and $A_c$ are respectively the concrete's Young's modulus and the section area of the concrete considered in the beam, $k$ and $L$ are respectively the slip modulus and the beam length. The structural stiffness is then calculated as follows

$$EI_{eff} = E_c\left(I_c + \gamma A_c a_c^2\right) + E_w\left(I_w + A_w a_w^2\right),\ a_w = \frac{\gamma E_c A_c (h_c + h_w)}{2(\gamma E_c A_c + E_w A_w)},\ a_c = \frac{(h_c + h_w)}{2} - a_w \tag{2}$$

where $a_w$ and $a_c$ are the distances between the centroid of a material and the effective neutral axis of the composite beam and $h$ is the member depth. Depending on the value of $\gamma$, which ranges from 0 to 1, the effective bending stiffness varies within the following two following bounds [38]:

$$EI_{\min} = E_c I_c + E_w I_w \tag{3}$$

$$EI_{\max} = \frac{EI_{\min} + (EA)^* r^2}{1 + \frac{\pi^2 (EA)^*}{kL^2}},\quad (EA)^* = \left(\frac{1}{E_c A_c} + \frac{1}{E_w A_w}\right)^{-1} \tag{4}$$

where $r$ is the distance between the rigidity's centroid of both layers. While the γ-method accurately predicts the load-deflection relationship in the serviceability limit states (SLS). It is also possible to predict the moment resistant at ultimate limit states (ULS) by reducing the slip modulus $k$ by an empirical factor of 2/3 [36]. The ULS prediction of the γ-method is merely empirical and its applicability should be verified as it may not well consider the effective stress redistribution at the structural collapse.

#### 2.1.2. Elastic-plastic methods

The frozen shear method [38] is based on the simplifying hypothesis of a connection with a perfectly elastic-plastic load-slip relationship. The estimated load-deflection curve is a bilinear function composed by an initial linear part based on the γ-method up to the plasticization of the external connectors, followed a second linear part with a reduced slope based on the hypothesis that all connectors have plasticized simultaneously (i.e., the shear force is frozen). The reduced stiffness slope can be simply calculated by considering the effective bending stiffness ($EI_{min}$) with zero composite action from Eq.(3). As a consequence, that the gradual plasticization of the connections is neglected, the frozen shear model tends to underestimate the structural response.

Frangi and Fontana [15] proposed an elastic-plastic model (EPM) to estimate the moment resistant of a composite beam by a simplified sectional analysis based on 3 assumptions, such as, (i) all the connectors plasticize (i.e., the shear force is equal to the maximum connection strength along all the beam); (ii) the stress distribution in the concrete section is linear for compression and negligible in tension; (iii) and finally the collapse is reached at the bottom fiber of the timber beam by a combination of tension and bending. Interestingly, they found that the EPM estimated moment resistant is approximately a linear function of the degree of composite action between two bounds given by moment with full composite action and the moment with no-composite action.

As the shear law $V$-$s$ of connections is not completely perfectly elastic-plastic, it is noteworthy to verify the applicability of existing ULS methods, such as, the Frozen Shear method and the Frangi's method, to predict the load-bearing capacity of the developed TCC structures.

#### 2.1.3. FEM model based on Newmark's composite beam theory

The numerical model is herein employed to verify the number of connections which have been fully yielded before the timber collapse as an important aspect of the developed ductile TCC structures which are plastically-designed to yield as many as possible ductile notch

connectors [19,22–23].

The governing differential equation of a composite beam made of two elastic beams with an horizontal shear force, which is linear with the interface slip, was first developed by Newmark [39] as follows

$$\frac{d}{dx}\left(\frac{1}{K_s}\frac{dN(x)}{dx}\right)-\frac{1}{C^*}\frac{EI_\infty}{EI_{min}}N(x)+\frac{d^2\Delta(x)}{dx^2}d=0 \tag{5}$$

where $C^*$ is a parameter of axial rigidity of the composite beam; $EI_\infty$ is the maximal composite bending stiffness; $N$ is the normal stress in each layer and $\Delta''$ is the second derivative of the beam deflection. Such equation can be solved numerically by Finite Element Method FEM and extended to inelastic material law with special numerical method [34,40–41]. Herein, we will employ a Finite Element code for TCC structures, namely DDuctileTCS®, which allows predicting the load-deflection curve of a TCC beam from a given non-linear shear connection law *V-s* as well as considering the effect of the tension damage (cracking) in the bottom side of the concrete slab under bending [34]. The TCC FEM model has been well validated against experimental tests on different TCC structures [30,34–35] and the numerical formulation and details can be found in [34]. As for the TCC FEM model, the differential Eq. (5) was discretized by means of 250 FEM composite beam elements of which element vector is described by 6 degree of freedoms (i.e., the displacement, rotation and the axial force of concrete and timber). All the FEM matrix and other numerical details are given in annexes of [34]. In particular, the employed TCC FEM model allows to directly consider the shear law *V-s* directly from the one which was experimentally measured by push-out tests as shown in the following Fig. 5 and described in section 5.1.

The mechanical property of the timber and concretes employed in FEM model agree with the ones presented in following section 4.1. Timber is assumed to behave elastically. Concrete is assumed to behave elastically in compression up to the compressive strength, while the tensile behavior is linear up the first-cracking strength, followed by a strain-hardening phase. As for HPC, the Young's modulus and the tensile strength of HPC (4.7 MPa) were assumed as explained in section 4.1, while the strain-softening part (after the peak strength) was neglected as no fiber reinforcement was employed. As for UHPFRC, the Young's modulus, compressive strength were measured in the laboratory, while the maximum tensile strength (8 MPa) was provided by the technical datasheet as described in section 4.1. Moreover, the first cracking strength and the deformation at the maximum tensile strength of UHPFRC were arbitrarily assumed to be 5 MPa and 0.1%, respectively, as rather reasonable for UHPFRC [42–43]. It is worth mentioning this assumption is not critical as it was found that the effect of post-cracking tensile law on the TCC inelastic behavior is rather secondary as concrete slab mainly works in compression and the internal stress redistribution of TCC structures also avoid crack localization in the concrete slab due to bending [34]. As verification, we have carried a parametric analysis by varying the 2 assumed values of the UHPFRC tensile law and observed that they have a very limited effect on the load-deflection curve. This is due to the fact that the.

## 3. Proposed multi-criteria design approach

This section presents the design of a simply supported TCC floor with a given span $L$ of 8 m, which can be considered as an optimal solution for timber multistory buildings in Canada. As for the design, we consider a simplified method [44] which considering the following criteria: (i) deflection caused by live loads; (ii) long-term deflection; (iii) vibration criterion; (iv) safety factor of the load-bearing capacity of the TCC structure; (v) structural ductility; (vi) total weight; (vii) floor thickness; (viii) fabrication cost; (ix) fire resistance and (x) the natural frequency. Based on the National Building Code of Canada (NBCC) [45], for office areas located in floors above the first storey the live loads (L) is 2.4 kPa, while the permanent loads (D), which includes the self-weight of the structure and an additional permanent load, is 1.5 kPa. The load combination for the ultimate limit state (ULS) is 1.25 $w_D$ + 1.5$w_L$.

For the serviceability limit state (SLS), both initial and long-term deflection were considered. The maximum admissible initial deflection caused by a uniformly distributed live load is $L$/360 as follows:

$$\Delta_L=\frac{5w_LL^4}{384EI_{eff}}\leqslant\frac{L}{360}\leqslant 22.2\ mm \tag{6}$$

where $w_L$ is the uniform live loads of 2.4 kPa; $L$ is the span of the beam and $EI_{eff}$ is the effective bending stiffness of the composite beam. For the total long-term deflection, the effect of creep of both materials as well the creep of the connection as considered [46–47]. Based on a simplified Adjusted Age Effective Modulus (AAMM) method the long-term deflection can be calculated by estimating a reduced bending stiffness $EI_{eff\_r}$ with reduced Young's moduli and the reduced connection stiffness as follows:

$$E_{CLTLT}=\frac{E_{CLT}}{1+\Phi_{CLT}};\ E_{UHPFRCLT}=\frac{E_{UHPFRC}}{1+\Phi_{UHPFRC}};\ E_{HPCLT}=\frac{E_{HPC}}{1+\Phi_{HPC}};\ K_{sLT}=\frac{K_s}{1+\Phi_{conn}}; \tag{7}$$

where creep coefficients used in this work are: $\Phi_{UHPFRC}$ = 0.8 for UHPFRC [48],$\Phi_{HPC}$ = 2 for HPC [49],$\Phi_{CLT}$ = 2 for CLT [50] and $\Phi_{conn}$ = 2 for the connection [7,47]. Based on NBCC, the total long-term deflection is composed by the initial deflection caused by live load and the long-term deflection caused by the permanent loads (i.e., the portion of sustained live load is not disregarded). Considering that the the NBCC admissible maximum deflection at long-term is $L$/180, the long-term deflection can be evaluated as follows

$$\Delta_{tot}=\frac{5w_LL^4}{384EI_{eff}}+\frac{5w_DL^4}{384EI_{effLT}}\leqslant\frac{L}{180}\leqslant 44.4\ mm \tag{8}$$

where $EI_{effLT}$ is the effective bending stiffness reduced to account creep of the composite beam.

The vibration criterion is based on the fundamental frequency $f_1$ of the composite beam which can be estimated as follows

$$f_1=\frac{\pi}{2L^2}\sqrt{\frac{EI_{eff}^{1m}}{m^{1m}}} \tag{9}$$

where $m^{1m}$ is the linear mass of the composite floor in kg/m for 1 m wide and $EI_{eff}^{1m}$ is the effective bending stiffness for a meter wide of the beam. Based on the Eurocode 5 [36], the fundamental frequency of should be higher than 8 Hz to be acceptable for a TCC floor. For lower frequencies between 6 Hz and 8 Hz, the solution can also be acceptable if the criteria below is respected [5,11]:

$$\frac{f_1}{d_{1kN}^{0.34}}\geqslant 6.23,\ d_{1kN}^{0.34}=\frac{10^6L^3}{48EI_{eff}^{1m}} \tag{10}$$

where $d_{1kN}^{0.34}$ is the deflection under 1kN point load in mm.

The safety factor of the load-bearing capacity is also considered, but such ULS state rarely governs the dimensioning of TCC floors in buildings. The safety factor $SF$ is defined as follows

$$SF=\frac{w_{max}}{w_{ULS}} \tag{11}$$

where $w_{max}$ is the maximum bearing load capacity estimated with the FEM non-linear Newmark method and $w_{ULS}$ is the factored load. Based on [44], the structural ductility (μ) is defined as follows

$$\mu=\frac{\Delta_u-\Delta_{EOL}}{\Delta_{EOL}} \tag{12}$$

where $\Delta_u$ is the maximum deflection and $\Delta_{EOL}$ is the deflection at the end-of-linearity in the load-deflection curve.

The fire resistance was calculated by assuming a one-dimensional char depth and a zero-strength layer in accordance to the Canadian standards [46,51]. A charring rate of 0.65 mm/min is used for the CLT and the zero-strength layer is 7 mm for a fire exposure duration of more than 20 min. A minimal fire resistance value of 2 h is needed. The load used in fire calculation is not factored and the mean strength of the CLT can be used in the calculations without any reductions according to CSA [51]. Note that, in order to obtain the mean strength of the CLT-$E_1$ stress grade, the specified strength from Table 2 has to be multiplied by an adjustment factor of 1.25 [51]. An iteration process was performed with the γ-method to determine the critical residual CLT cross-section which withstands the unfactored load with the mean strength. The charring rate and the zero-strength layer are used to determine the critical time under fire needed to reduce the CLT to the critical cross-section thickness. As the layer of concrete is considered protected by the CLT, no reduction to the concrete of the connection is applied. For sake of safety, the stiffness of the only CLT is considered.

Finally, the floor weight and the floor thickness are also considered because of practical importance. The construction cost was estimated based on approximate price in Canada, i.e., the cost of CLT was chosen equal to 850 \$/m$^3$, the cost of UHPFRC was assumed to be equal to 3000 \$/m$^3$, the cost of HPC was estimated to be equal to 300 \$/m$^3$. As for the connector, the cost was estimated to be 10 \$/conn by considering the CNC time needed and the screws.

Based on the material property presented in the following section 4.1, Fig. 1 shows the results of the multi-criteria design of the optimized CLT-UHPFRC and CLT-HPC configuration for the chosen concrete thickness. For instance, by considering the CLT with 5 timber layers produced by industrial partner (Table 2), the UHPFRC thickness was estimated by the multicriteria design approach (Fig. 1). For instance, it was necessary a UHPFRC thickness of 55 mm to assure the vibrational criteria is greater than 6.3 based on Eq. (10).

Table 2 Summarizes the section of CLT-HPC and CLT-UHPFRC composites slabs.

## 4. Experiment

### 4.1. Material properties

The employed Cross Laminated Timber (CLT), which is commercially available under the name of Nordic X-Lam 175-5 s [52], is composed of 5 layers of 35 mm with a total thickness of 175 mm. As reported in Table 1 [52], the mean mechanical properties have been estimated from the design (characteristic) values of the CLT technical sheet [52] by considering the factor (1.25) for passing from design to mean values for CLT as suggested by CSA O86 as well as the short-term duration factor (1.15). In addition, the CLT effective stiffness $(EI)_{eff}^{CLT}$ which includes the rolling shear compliance based on the shear analogy method is reported [53], which corresponds to a effective elastic modulus of $Ew = 9.2$ GPa as employed in the following calculation. Owing to the high slenderness of the CLT the shear effect on the deflection are negligible [54]. The reported net global warming potential −591 kg of $CO_2$ eq./m3 of CLT.

The employed Ultra High-Performance Fiber Reinforced Concrete (UHPFRC), which is commercially available under the name UP-F2 by King Materials, includes a volume content of 2% of steel microfibers with a length of 12.7 mm and a diameter of 0.2 mm. The compressive strength and the Young's Modulus $E$ of both concrete were tested in laboratory accordingly to the ASTM C39-18 M [55] and the ASTM C469M-14 [56]. The employed High-Performance Concrete (HPC) is a premix product which is available under the commercial name of HP S10 by King Materials. Alternatively, a ready-mix HPC with equivalent property which was also employed with a water-to-cement ratio of 0.31. Table 2 summarizes the mean values and standard deviation of the mechanical properties of the concretes which were characterized

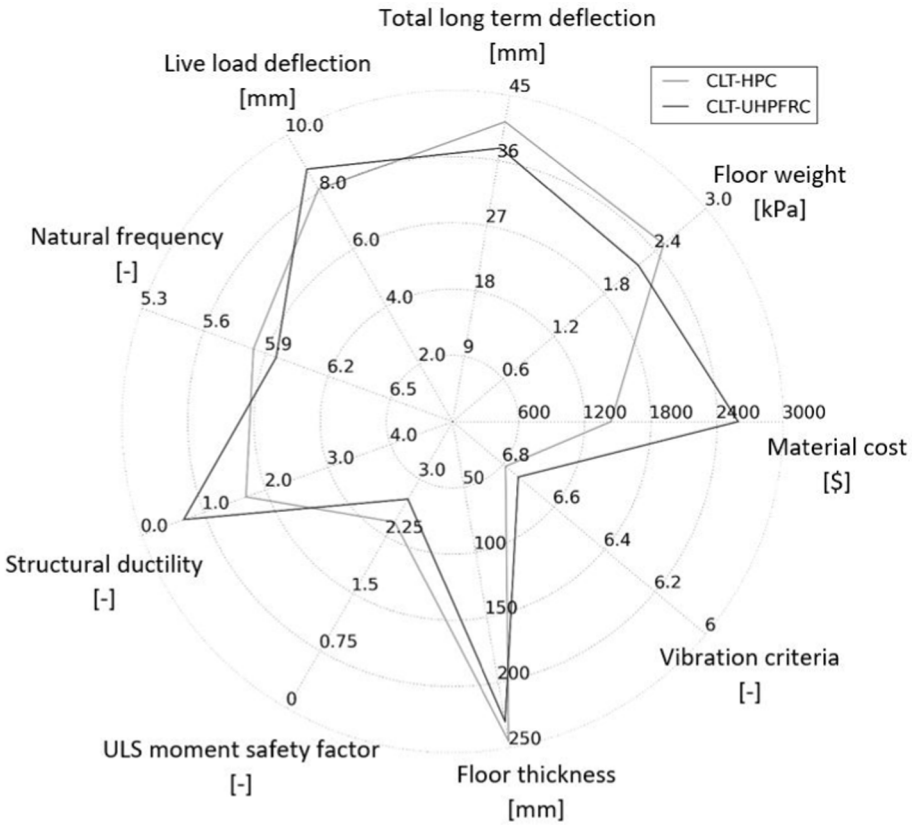


**Fig. 1.** Radar view of the considered design criteria for the two composite floors CLT-HPC and CLT-UHPRC.

**Table 1**
Predicted results for both configurations.

| TCC slab | Cost [$/m$^2$] | Total weight [kPa] | Long term deflection [mm] | Live load deflection [mm] | Natural frequency $f_1$ [Hz] | Structural ductility $\mu$ [–] | Safety factor SF [–] | Floor thickness [mm] | Vibration [Hz] |
|---|---|---|---|---|---|---|---|---|---|
| CLT-HPC | 1612 | 2.5 | 41.3 | 8.1 | 5.84 | 1.69 | 2.00 | 245 | 6.79 |
| CLT-UHPFRC | 2596 | 2.2 | 37.7 | 8.8 | 5.95 | 0.67 | 2.40 | 230 | 6.74 |

**Table 2**
Mechanical properties of the materials tested.

| Component | Product | E [GPa] | $(EI)_{eff}^{CLT}$ [N·mm/m $10^9$] | $f_b$ [MPa] | $f_t$ [MPa] | $f_c$ [MPa] |
|---|---|---|---|---|---|---|
| CLT Beam | X-Lam 175–5 s | 11.7 | 4140 | 40.5 | 22.1 | 20.7 |
| UHPFRC | UP-F2 | 41.2 ± 1.0 | – | – | 8.0 | 119.6 ± 4.1 |
| HPC (premix) | HP-S10 | 36.0 ± 2.2 | – | – | 4.7 | 64.7 ± 2.3 |
| HPC (ready-mix) | – | 30.1 ± 0.2 | – | – | 4.0 | 63.6 ± 1.2 |

experimentally with the exception of the UHPFRC tensile strength which was taken from the technical datasheet of the industrial partner [57].

### 4.2. TCC beams

The notches were cut out from the CLT slab by means of a computer numerical control (CNC) machine. Based on a previous experimental campaign where several notch configurations were tested by push-out tests [23], the notch connection CLT-25-2 and CLT-20-2 were employed for UHPFRC and for HPC, respectively (where in the code CLT-XX-Y, XX stands for the notch depth, and Y for the number of additional screws). Fig. 2 shows both floor configuration with 8 notch connectors with a spacing varying between 700 and 900 mm. Additional screws (which are commercially available under the name of MyTiCon VG-plus 8 mm × 180) were positioned in the notches to avoid possible uplift. The screw head was positioned at mid height of the concrete

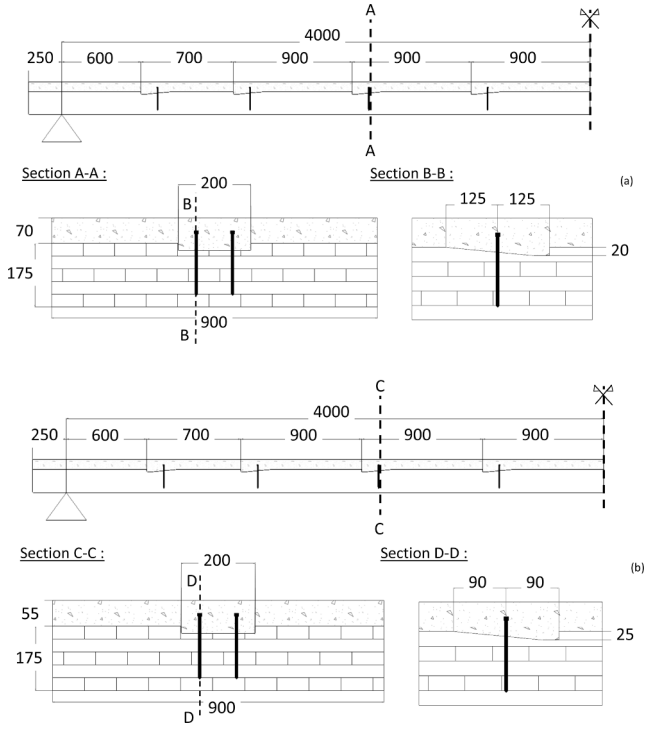


**Fig. 2.** Tested TCC floors: (a) CLT-HPC; (b) CLT-UHPFRC (units in mm).

layer. UHPFRC was cast in the longitudinal direction to favor the fiber alignment. A plastic film was laid over the concrete after casting to avoid plastic shrinkage. After 24 h of curing, a curing blanket was placed over the floor samples for 6 extra days to avoid shrinkage cracking. Then, specimens were cured for 28 days in laboratory conditions before testing.

In order to consider the effect of two possible shoring configurations at the construction site, two different casting methods were considered: (i) 3 composite slabs, CLT-HPC#1, CLT-HPC#1 as well as CLT-UHPFRC were cast on 3 supports system with uniform clearance span of 4 m to simulate the use of a single shoring at mid-span during construction. For CLT-HPC#1 and CLT-HPC#2, a polyethylene film was laid over the CLT and held into the notch with staples to protect it from wetting. No plastic sheet was employed for CLT-UHPFRC as a water exchange is unlikely due to the low water content, the extremely low permeability and rapid hardening of such concrete. The middle support was taken off after 7 days; (ii) CLT-HPC#3 and CLT-HPC#4 were cast on the floor to represent a large number of shoring during concrete hardening. Contrarily to the previous case, no plastic film was employed for CLT-HPC#3.

### 4.3. Push-out tests

The push-out tests were carried out with a test set-up with an eccentric configuration (Fig. 3a), which has the advantage to reduce the sample size, but the engendered transversal force can cause a slight overestimation (e.g., 5–10%) of the maximum shear strength and connection stiffness [36,58]. The load was applied according to the EN 26,891 standard [59] as shown in Fig. 3b. Two LVDTs were installed on both sides of the specimen to measure the relative slip between the concrete and the timber at the notch position. Teflon plates were attached to the steel frame to reduce the friction. Full details of the test set-up can found in [23].

The CLT timber samples were 175 mm, 700 mm and 1000 mm in height, length and width, respectively. The notch configuration was carved in about 30 s with a 100 mm diameter drill bit and finished with a precision drill bit of 40 mm diameter in the factory of the industrial partner. The actual shape of the notches is shown in Fig. 2 B-B and D-D for HPC and UHPC, respectively. In more details, for CLT-HPC samples, the notch dimensions were 250 mm, 200 mm and 20 mm in width in height, length and width, respectively. For CLT-UHPFRC samples, the notch dimensions were 180 mm, 200 mm, and 25 mm in width in height, length and width, respectively. Such notch dimensions were selected based on the connection properties (stiffness, strength and ductility) measured by a wide campaign of push-out tests, where 14 different

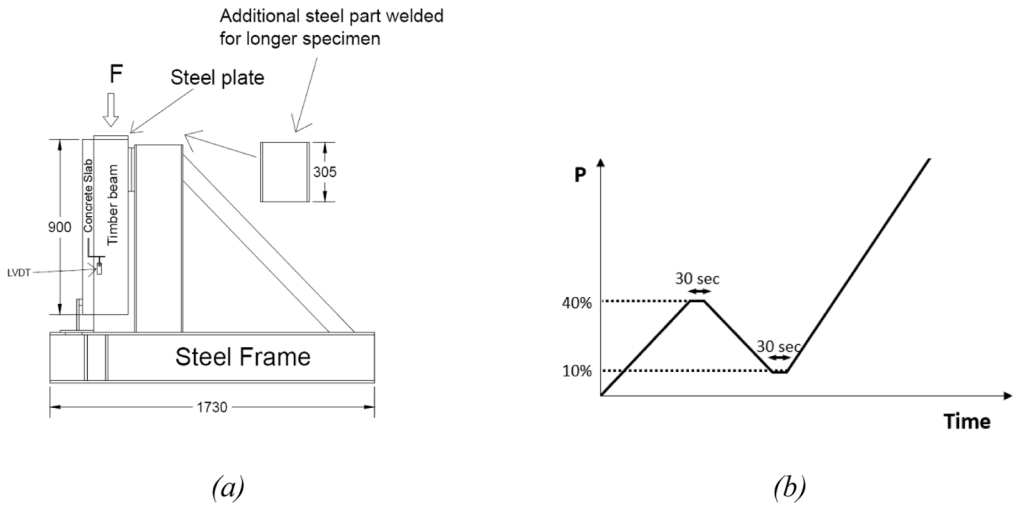


**Fig. 3.** (a) Loading protocol for the push-out test; (b) Lateral view of the push-out test set-up.

configurations were considered (see full details in 23). In particular, the connection configurations with acronym CLT-20-2 and CLT-25-2 in that study have been herein employed for CLT-HPC and CLT-UHPFRC, respectively. The connection samples were tested within 47–62 days after casting (based on the laboratory availability of the mechanical press), which allows concrete to achieve their hardened properties. Six tests were performed for both connection type.

### 4.4. Flexural bending test setup and measurement of natural frequencies

Fig. 4a shows the test set-up of the bending test with 4 loading points which is similar to the one employed in previous works [44,59–60]. The deflection was measured at the mid-span center by two potentiometers supported by an aluminium yoke, which filters out the possible timber deformation at the support. Four Linear Variable Differential Transformers (LVDT) were used to measure the slip between the concrete slab and the CLT on both sides of the beam at both supports.

The loading test control was divided in 2 steps as shown in Fig. 4b. During the first step, the deflection $\Delta$ is increased at a rate of 8 mm/min up to 30% of the maximum load, which represent a bending moment similar to the SLS condition. This displacement is maintained for 30 s. The load was reduced to approximately 10% of the estimated maximum load $P_{max}$ and maintained for another 30 s. Then, the load was increased to $0.4\ P_{max}$. After this point, the displacement was increased to a rate of 10 mm/min up to the collapse of the TCC beam.

In order to measure the natural frequencies of the TCC beams a classical impact-response test, which is also called a modal test, was performed [50]. Seven accelerometers were fixed at a uniform distance along the beam length under the CLT to estimate the 1st and 2nd order frequency and the damping ratio of the first natural frequency. The hammer used during the test was a 2.5 kg Kistler model no. 9278A with a soft tip which creates a long impact duration in the low frequency. The accelerometers used for the acquisition had an operating range of 0.2–1000 Hz and a sensitivity of 500 mv/g. The data acquisition and the processing were done with software named LMS Test.Lab Impact Testing. This method provides a first order estimation of the unidirectional vibrational mode, although bidirectional vibrational mode may be more suitable for CLT-concrete floor [61].

## 5. Results and discussion

### 5.1. Push-out test results

Fig. 5a and b show the shear connection law of the notch connections for CLT-HPC and CLT-UHPFRC, respectively. The CLT-HPC exhibited a mean connection stiffness $K_s$ of 351 ± 52 kN/mm and maximum shear strength $V_{max}$ of 143.8 ± 18.3 kN. The CLT UHPFRC exhibited a mean connection stiffness $K_s$ of 398 ± 22 kN/mm and maximum shear strength $V_{max}$ of 198.5 ± 13.8 kN. The UHPFRC slab has a higher connection stiffness and maximum shear strength because the higher notch depth of 25 mm instead of 20 mm for the CLT-HPC connection. Both connections exhibited a remarkable ductile behavior in terms of shear load vs. slip. The collapse of the CLT-HPC connection was characterized by a shear failure of the concrete after the plasticity of timber grains in longitudinal compression. The collapse of CLT-UHPFRC connection was characterized by a shear failure of the steel screw

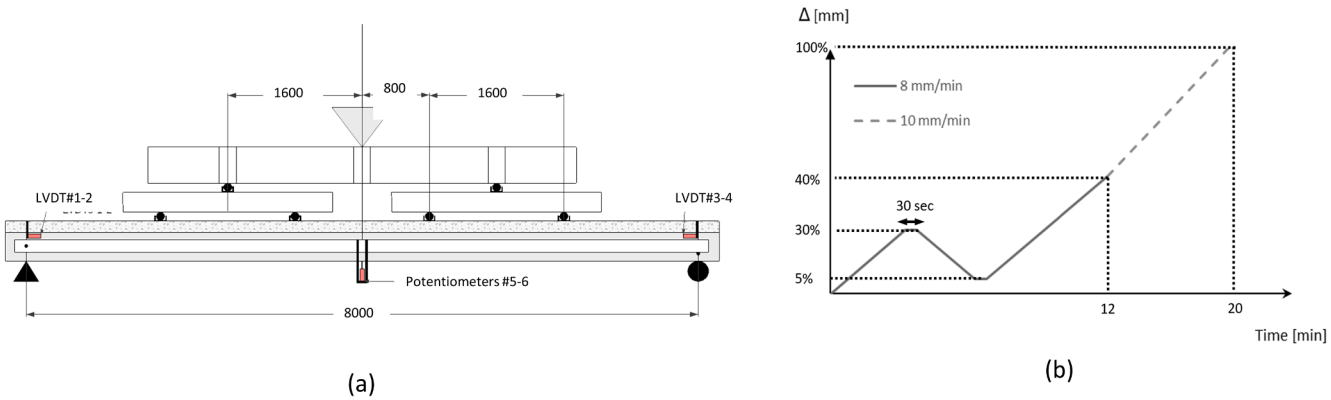


**Fig. 4.** (a) Flexural bending test set-up with 4 points load: (b) Test control for the bending tests.

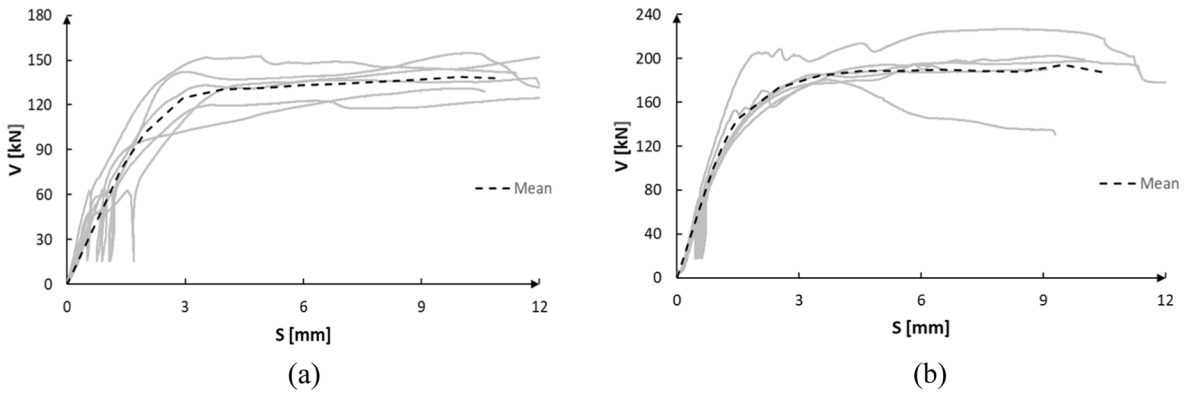


**Fig. 5.** Shear-slip curves of the connection for (a) CLT-HPC and (b) CLT-UHPFRC.

after the plasticity of timber grains in longitudinal compression. Full details and photos of the failure modes can be found in [23].

### 5.2. Static bending test results

Fig. 6 shows a photo of bending tests on a CLT-UHPC floor in the laboratory. Fig. 7 presents the experimental flexural response of CLT-HPC floor systems in terms of load-deflection curves *P-Δ* with indication of the SLS and ULS loads. The experimental response is also compared with the the simulated response by FEM and the ones estimated by the aforementioned existing simplified methods. Table 3 reports also the deflection at ELS load, the initial structural slope $dP/d\Delta$, the load $P_{EOL}$ and displacement $\Delta_{EOL}$ at the end of linearity, and the structural ductility $\mu$ as defined above. In summary, the deflection limits and the structural ductility are satisfactory. While the experimental responses of all CLT-HPC floors satisfy the ULS deflection limit ($L/180 = 44$ mm) and ULS safety factor (which is about 2.2), their flexural response is less stiff than the one estimated by the existing methods and FEM analysis. Moreover, CLT-HPC#1 and #2 composite slabs showed a less stiff than the CLT-HPC#3 and #4. In particular, the CLT-HPC#2 exhibits a more symmetric behavior in terms of slip on the two side of the beams, which favors a slightly stiffer structural behavior than CLT-HPC#1. Notably, the beam CLT-HPC#3 and CLT-HPC#4 which were cast on the ground and without the plastic sheet exhibited a stiffer structural response. Finally, the maximum load for CLT-UHPC calculated with the Frangi method which assumes that all connectors yield at Vmax of 198.5 kN is 195 kN. The difference with the experimental maximum load may be explained by the fact that not all connectors have yielded or to possible inelastic effects (e.g., shear concrete cracking in notch or notch uplift) occurring at higher load.

Fig. 8 presents the experimental flexural response in terms of load-deflection *P-Δ* for the CLT-UHPFRC. The CLT-UHPFRC slab exhibited a stiff response as expected. Interestingly, the TCC system was able to redistribute the load after the first load drop at 120 kN due to a wood slat breaking (Fig. 9a) and the final failure occurs at 170 mm, when timber broke in tension. The CLT-UHPFRC slab verifies the ELS deflection and its ULS safety factor is about 2.4 (Table 5). The γ-method well predicts the initial elastic response of the composite floor, but it does not well capture the inelastic response. The Frozen method well predict the initial elastic response, while it captures the inelastic response in an average manner. The experimental response is well in agreement with the simulated one by FEM up to the first load drop. Finally, the maximum load for CLT-UHPC estimated with the Frangi method is estimated to be 200.1 kN with assumption of all connector yield at Vmax

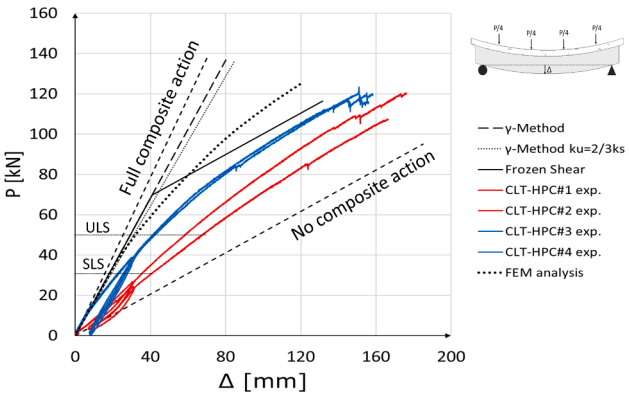


**Fig. 7.** Comparison of the experimental load-deflection P-Δ curves with the ones estimates by simplified methods for the CLT-HPC slabs.

**Fig. 6.** Photo of a bending test on a CLT-HPC floor in the laboratory.

**Table 3**
Flexural test results.

| TCC slab | $\Delta_{SLS}$ [mm] | $\frac{dP}{d\Delta}$ [kN/mm] | $P_{EOL}$ [kN] | $\Delta_{EOL}$ [mm] | $P_{MAX}$ [kN] | μ [–] |
|---|---|---|---|---|---|---|
| CLT-HPC#1 | 43.1 | 0.75 | 38.9 | 52.2 | 109 | 2.24 |
| CLT-HPC#2 | 37.4 | 0.85 | 54.7 | 64.2 | 121 | 1.76 |
| CLT-HPC#3 | 27.4 | 1.20 | 48.1 | 40.0 | 117 | 2.84 |
| CLT-HPC#4 | 27.3 | 1.20 | 48.1 | 40.0 | 120 | 2.95 |
| CLT-UHPFRC | 25.6 | 1.31 | 55.8 | 42.6 | 120 | 2.95 |

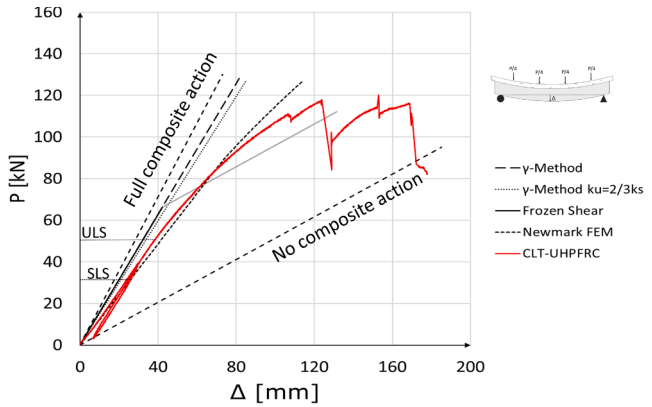


**Fig. 8.** Comparison of the experimental load-deflection P-Δ curves with the ones estimated by simplified methods for the CLT-UHPFRC slab.

of 198.5 kN. While Frangi method provides an upper bound of the ultimate load, it seems possible to increase the ultimate load if all connectors are allowed to yield before concrete collapse if any additional inelastic effects at high loading are avoided (e.g., concrete shear cracks at the notch corners or notch uplift). Considering recent results on timber-concrete composite slabs with different shear reinforcement in the concrete notches [25], it is also possible that end-to-end vertical connection which avoid any uplift at high loads are necessary.

To check the potential factors which have affected the low structural stiffness of CLT-HPC#1 and CLT HPC#2, both slabs were cut in half as shown in Fig. 9b. Additionally, a reference beam of CLT-HPC slab (called CLT-HPC#1-2ref) was cast and cured as CLT-HPC#1 and CLT-HPC#2 and cut for inspection without testing. Two major issues were found which could explain the lower structural stiffness of the system CLT-HPC#1 and CLT-HPC#2, such as: (i) the contact area between timber and concrete was not completely filled due to the plastic sheet (Fig. 9c). Thus, the notch did not work the entire depth of the connexion as it was designed to [62]. The plastic sheet did not allow the concrete to fill the notch resulting in a rounded shape as shown in Fig. 10a; (ii) a diagonal crack was visible in the concrete slab in the proximity of the notch corner. This crack was likely formed during the shrinkage effect of the slab over the supports.

The effective depth of the notch was measured on the slab CLT-HPC#1-2ref with a digital caliper for all notches by looking at the vertical proportion of the notch. Fig. 10b shows the effective depth $D'_n$ which was measured on all the notch of the cut sections for slab CLT-HPC#1-2ref. It was estimated that the real effective average depth was 10 mm instead with a standard deviation of 2.4 mm instead of the 20 mm

In order to account for the reduction of contact area due to the plastic sheet, the connection law V-s was reduced by a factor equal to $D'_n/D_n$. Fig. 11.b and c show the experientially measured shear law V-s and the effective one by employing the multiplicative reduction factor $D'_n/D_n$. To test this hypothesis, the structural response with the reduced shear law V-s was calculated with the non-linear FEM model (63). Fig. 9b

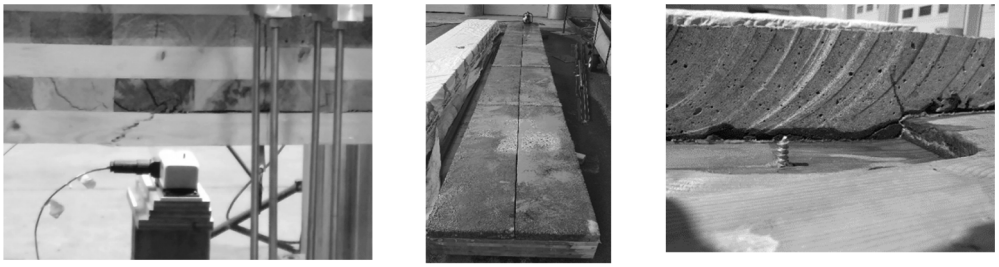


**Fig. 9.** (a) Broken slat observed at the first load-drop at 120 kN for slab CLT-UHPFRC; (b) Cut performed on concrete slab CLT-UHC#1, #2 and #1-2ref; (c) Photo of a notch connection section with concrete crack and not complete filling of the notch.


**Fig. 10.** (a) Photo of the rounded shape of the concrete notch due to the plastic film; (b) Definition of the reduced depth $D'_n$ of the notch.

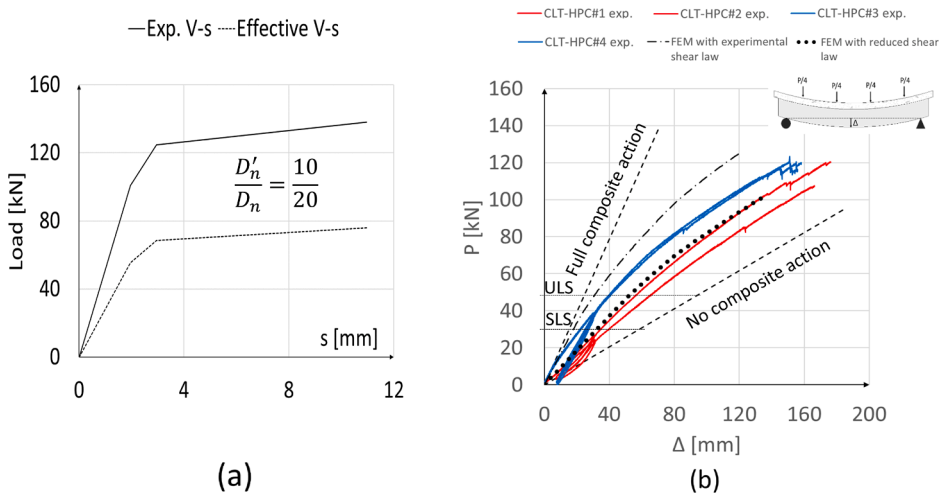


**Fig. 11.** (a) Experimental and reduced shear law for the CLT-HPC notch connector; (b) Comparison between the experimental and simulated load-deflection curve.

compares the load-deflection curves of the experimental tests with the one estimated with the reduced shear-law. The correction factor allows to predict very well the experimental structural behavior of the beams CLT-HPC#1 and #2 in term of load-deflection. Thus, the reduction of contact area can then explain the lower structural stiffness of slab CLT-UHPFRC#1 and #2. In summary, the FEM model confirmed the issue of shear connection reduction for slab CLT-UHPC#1 and #2 as, due to the use of plastic sheet waterproof, the notch was not completely filled by concrete with a reduction of the contact area.

On the other hand, the FEM simulated results with the real experimental shear law *V-s* better compare with the experimental structural response of beams CLT-HPC#3 and #4, for which the plastic sheet was not employed and the casting was performed on the ground. However, there is still a slight difference between the experimental response of CLT-HPC#3 and#4 and FEM simulated results with experimental shear law. As the notch contact area was not affected by the use of a plastic sheet, this stiffness reduction can be explained by the second observed factor, i.e., the diagonal cracks in the concrete slabs observed at the notch corner (Fig. 9b).

Finally, the maximum load for CLT-HPC estimated with the Frangi method is estimated to be 172 kN in the case that all connectors have yield at reduced Vmax of 71.9 kN. Yet, possible notch uplift or shear crack in the concrete notch may have occurred at high loading.

### 5.3. Slip behavior results

As it is critical for a plastically designed TCC structures that all the connectors should yield before the timber beam collapse in a brittle manner, this section investigates the experimental slip distribution and estimates the shear distribution along the timber-concrete interface at different loading levels.

As observed in previous works [44,60]), the slip distribution is symmetric during the elastic phase of the connection, but it becomes asymmetric at higher load. On of the possible reasons is that not all connectors have exactly the same strength in reality and that slip tends to localize along the zone with weaker connection strength. Fig. 12a shows the load-slip curves for all tested slabs with distinction with North (N) and South (S) beam end (P-s). The FEM model assumes a uniform and symmetric property distribution of connector property, which induce a symmetric slip behavior at both ends of the slab. The FEM analysis provides a good approximation of the slip distribution for the CLT-HPC#2 slabs because this test was characterized by a more symmetric slip behavior. The CLT-HPC#1 was characterized by a weaker connector on the South end which causes large slip occurring on South side and small on North side. For the Slab CLT-HPC#2, #5 more LVDTs were installed on the composite slab to measure the slip at 1, 2, 4, 6, and 7 m in addition to the LVDT's at both ends. Three load levels were identified on each curve, such as: (*A*the end of linearity (EOL); (*B*) an intermediary point between *A* and *C*; (*C*) the failure load.Fig. 13

The FEM model with the reduced connection law well reproduces the slip observed along the slab CLT HPC#2 and CLT-HPC#4 as shown in Fig. 11a and 11b, respectively.

It is possible that some internal connectors remain elastic, but nevertheless the beam exhibits inelastic behaviour. In general, the

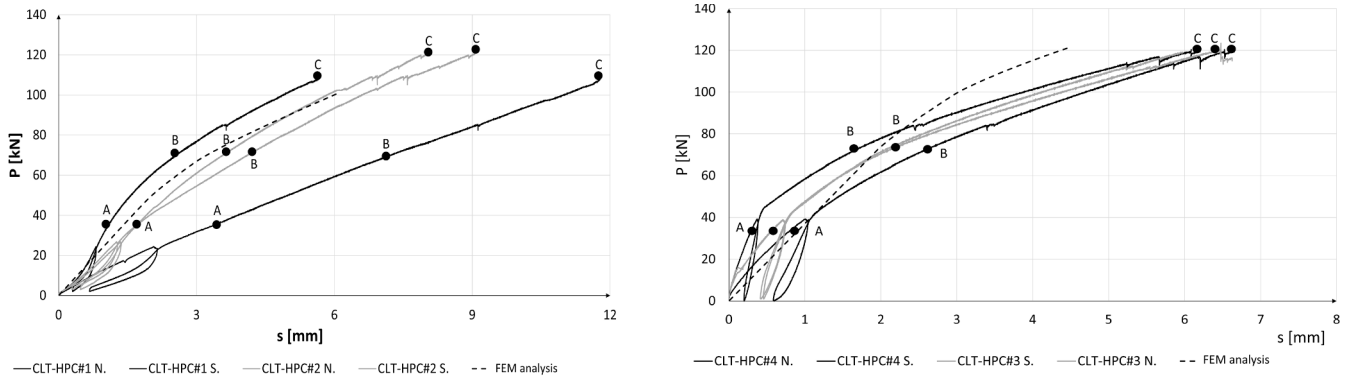


**Fig. 12.** Load-slip curves for slabs: (a) CLT-HPC#1 and #2; (b) CLT-HPC#3 and #4.

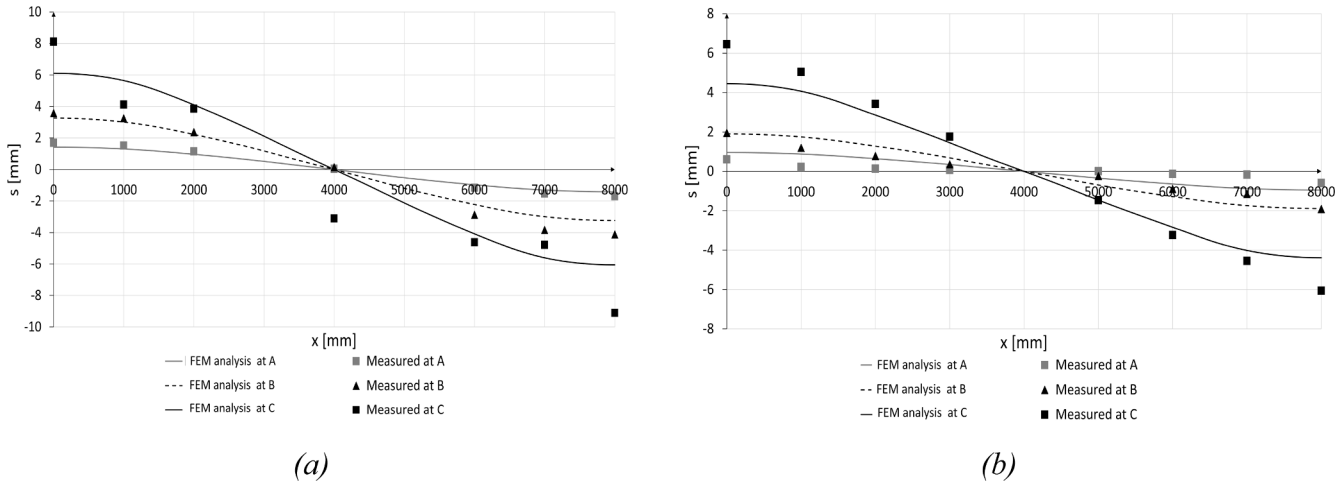


**Fig. 13.** Slip distribution a different load levels for slabs: (a) CLT-HPC#2; (b) CLT-HPC#4.

greater is the numbers of connectors which fully yield and undergo to inelastic deformation, the greater structural ductility would be.

Finally, the slip relationship can be transformed in shear with the experimental connection law *V-s* of Fig. 5. Fig. 14a and 12b compares the FEM simulated and experimental shear stress distribution at different load levels for CLT HPC#2 and CLT-HPC#4, respectively. With the exception of the asymmetric behavior in the middle of the slab observed at the end of the test for CLT-HPC#4, the shear distribution is fairly well predicted by the FEM model. One can observe that at the peak load most the connectors have yielded up to about ¾ of the half beam length.

By considering the experimental connection law without any correction factor (Fig. 4b), Fig. 15 compares the experimental and simulated load-slip curves for the CLT-UHPFRC. The slip distribution was rather symmetric up to the peak load. The FEM well captures the experimental load-slip response with a slight underestimation of the slip at the peak load.Fig. 16

Fig. 14a compares the slip distribution at the different load levels. Yet, the comparison between the simulated and experimental slip distribution is rather satisfactory for load level *A* and *B*, while the simulated values tends to slightly underestimate the slip distribution at the peak load *C*. This can be explained by the aforementioned overestimation of the connection law due to the asymmetric test set-up.

Fig. 14b compares the shear force distribution along the slab (by transforming slip to shear by means of the connection law (Fig. 5b). Most of the connector yield at the peak load C up to about ¾ of the half beam length.

### 5.4. Vibration test results

The modal test was repeated several times by moving the point of impact. Table 4 presents the modal results. The measured first order frequency fits with the predicted value with an average error of 10% between the measured values and the ones calculated with the Eq. (9). Interestingly, the measured natural frequency well corresponds to the calculated ones with a slight overestimation of less than 10% without the need to account for any reduction of the connection stiffness. The reason is that the vibrational behavior depends on small frictional forces between the CLT and the concrete interface. The measured dumping ratio is also low 1% for all slabs indicating negligible inelastic behaviour.

## 6. Conclusion

This works introduces an innovative composite slab made of CLT-HPC and CLT-UHPFRC with the use of ductile notch connectors by a methodology which combines structural design and experimental validation of simulated results. Based on the presented results, the following conclusion can be drawn:

1. For both CLT-HPC and CLT-UHPFRC slabs, the criteria of the vibration and the long-term deflection governed the design. As expected for TCC structures designed for residential applications, the moment strength is significantly overdesigned;
2. As for the CLT-HPC slabs, 2 fabrication procedures were considered to represent different constructions situations. The slabs CLT-HPC#1

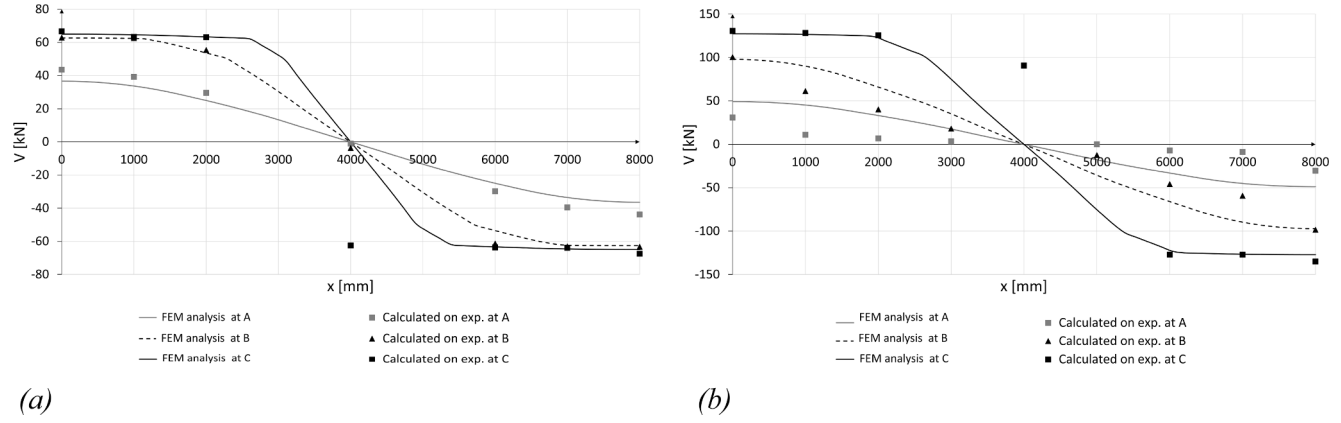


**Fig. 14.** Shear flow distribution for slabs: (a) CLT-HPC#2; (b) CLT-HPC#4.

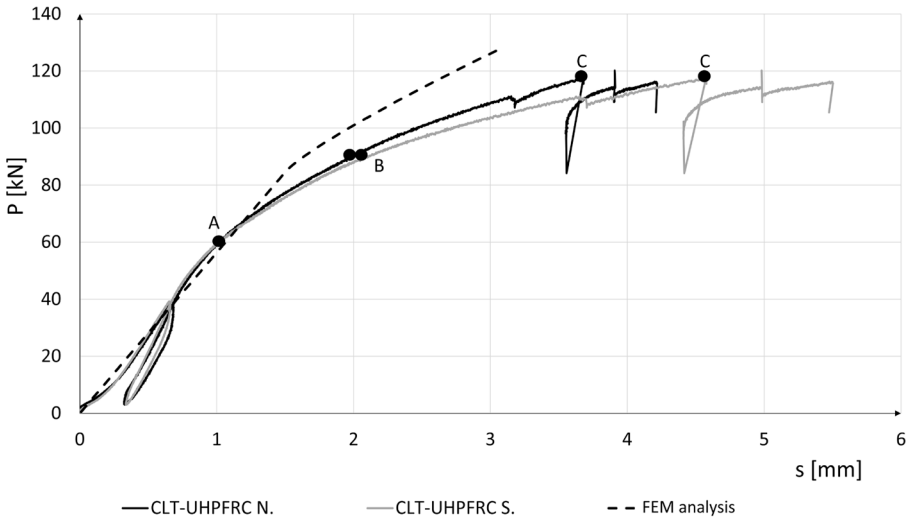


**Fig. 15.** Comparison of the expeimental and simulated load-slip curves for the CLT-UHPFRC composite slab.

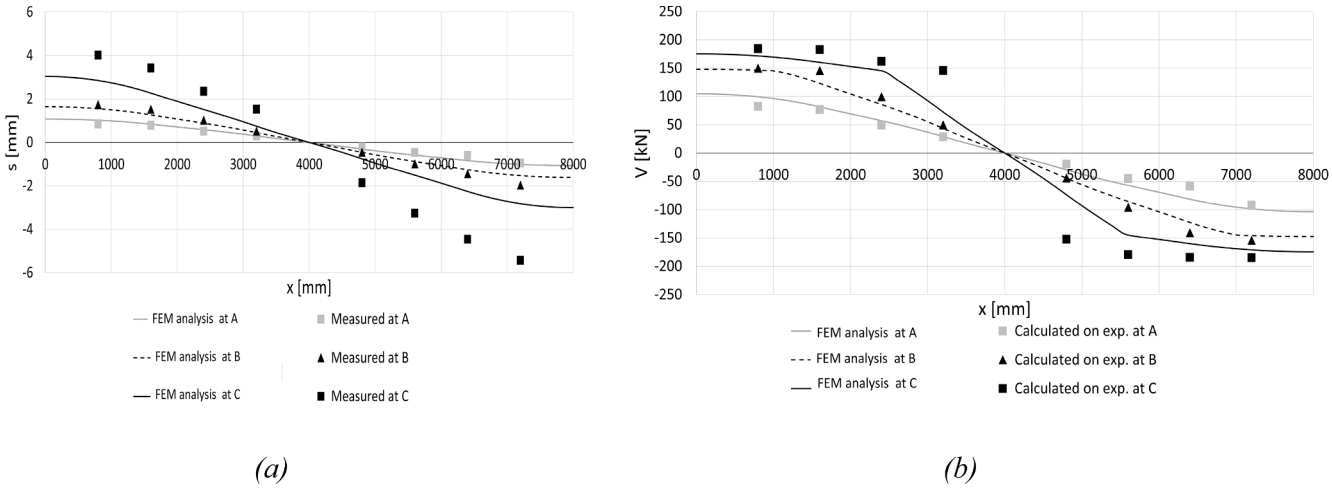


**Fig. 16.** (a) Slip between the UHPFRC and the CLT at different positions on the slab; (b) Horizontal Shear distribution along the CLT-UHPFRC.

**Table 4**
Calculated and Average measured results of the natural frequency.

| TCC slab | Measured $f_1$ (Hz) | Predicted $f_1$ | Difference (%) | Measured $f_2$ (Hz) | Measured damping ratio for $f_1$ (%) |
|---|---|---|---|---|---|
| CLT-UHPFRC | 6.5 | 5.95 | 3.6 | 21.3 | 1 |
| CLT-HPC#1 | 6.4 | 5.84 | 6.1 | 17.2 | 1 |
| CLT-HPC#1 | 5.9 | 5.84 | 15.0 | 18.0 | 1 |

and #2 were cast with plastic sheet waterproofing between the CLT and the concrete on 3 supports (e.g. 1 single shoring at mid-span). Their structural response was less stiff than expected due to a loss of contact area at the notch connection. Differently, slabs CLT-HPC#3 and #4 were cast on the ground without a plastic sheet between the CLT and concrete. Their structural response was stiffer and closer to the one expected. Still, the slight mismatch may be likely due to diagonal cracks which occurred in the HPC slab at the notch corner. It is recommended that a shear reinforcement or steel fibers are added to the concrete slab at the notch location to avoid this kind of cracking;

3. As for the CLT-UHPFRC slab, the structural behavior was stiff at low load and allows yielding of the connectors with a remarkable deflection at failure (~L/48). No diagonal cracks were observed in the notch corner of the UHPFRC slab thanks to steel fiber reinforcement;
4. The measured slip distribution was fairly well in agreement with the predicted values of the FEM modeling at different load levels. Such results confirm that the CLT-HPC and CLT-UHPC were *plastically designed* to allow most of the connectors to fully yield before timber collapse. In particular, based on FEM analysis, the ductile connectors fully yield over a length of 50% and 37% of the half beam length for CLT-HPC and CLT-UHPFRC beams, respectively. For plastically designed TCC structures, it is then recommended to dispose the ductile connectors on the external beam side for at least ¾ of the half-beam length;
5. The FEM modeling was also employed to better understand the effect of the plastic sheet waterproofing which reduced the notch contact

area for beams CLT-UHPC#1 and #2. By assuming a reduction of the shear connection force which is proportional to the observed reduction of the notch contact area, it was possible to predict the reduced structural stiffness which was observed in the bending tests;
6. The simplified γ-method with effective CLT elastic modulus based on shear analogy method is well suited to model the linear elastic response of CLT-HPC and CLT-UHPC floor. However, CLT-HPC and CLT-UHPC did not achieve the maximum load estimated by Frangi's upper bound method. For floor applications, this is not an issue as the safety factor on the ultimate limit state (ULS) load is considerably high. A recent work of composite timber-concrete slab evinced the importance of adding end-to-end vertical notch connections which avoids notch uplift at high load [25];
7. A CLT-UHPFRC floor with a slenderness ratio of 35 and light weight (2 kPa) was designed based on the governing design criteria of vibration and deflection and validated in laboratory. Neither the shear reinforcement for the notch connections nor the plastic sheet between timber and concrete were required.

Future work is needed to understand the effect of concrete shrinkage on the TCC structural behaviour as well as predicting the long-term deflection. Moreover, on-going works are now verifying the water exchange between timber and UHPFRC and whether or not a sheet waterproofing is required.

## CRediT authorship contribution statement

**Serge Lamothe:** Writing - original draft, Methodology, Visualization. **Luca Sorelli:** Conceptualization, Writing - review & editing. **Pierre Blanchet:** Supervision, Writing - review & editing. **Philippe Galimard:** Supervision, Writing - review & editing.

## Declaration of Competing Interest

The authors declare that they have no known competing financial interests or personal relationships that could have appeared to influence the work reported in this paper.

## Acknowledgements

The authors are grateful to Natural Sciences and Engineering Research Council of Canada for the financial support through its ICP and CRD programs (IRCPJ 461745-12 and RDCPJ 445200-12) as well as the industrial partners of the NSERC industrial chair on eco-responsible wood construction (CIRCERB) and the Quebec's Economy and Innovation ministry. The authors would like to acknowledge Mr. Keven Durand and Ms. Julie Frappier of Nordic Engineered Wood for the donation of the CLT as well as Mr. Julien Peña Cruz of King Materials for the donation of the UHPFRC mix materials and assistance during the casting. We also thank Mr. Jean-Philippe Letarte of MyTiCon for the donation of screw connections. We also would like thank MyTiCon for providing the screws employed in this work.

## References

[1] Smith I, Frangi A. Use of timber in tall multi-storey buildings. International Association for Bridge and Structural Engineering (IABSE). 2014.
[2] Brandner R, Flatscher G, Ringhofer A, Schickhofer G, Thiel A. Cross laminated timber (CLT): overview and development. Eur J Wood Wood Prod 2016;74(3):331–51.
[3] Dias A, Skinner J, Crews K, Tannert T. Timber-concrete-composites increasing the use of timber in construction. Eur J Wood Wood Prod 2016;74(3):443–51.
[4] Connolly T, Loss C, Iqbal A, Tannert T. Feasibility study of mass-timber cores for the UBC tall wood building. Buildings 2018;8(8):98.
[5] Hu L, Cuerrier-Audair S, Chui YH, Ramzi R, Gagnon S. Design method for controlling vibrations of wood- concrete composite floors systems 2016;9.
[6] Auclair-Cuerrier S, Sorelli L, Salenikovich A, Fafard M. The effect of rotatory inertia on the natural frequencies of composite beams. J Sound Vib 2016;366:230–47.
[7] Yeoh D, Fragiacomo M, De Franceschi M, Heng Boon K. State of the art on timber-concrete composite structures: Literature review. J Struct Eng 2010;137(10):1085–95.
[8] Lukaszewska E. Development of prefabricated timber-concrete composite floors. Luleå tekniska universitet 2009.
[9] Hassan OA, Öberg F, Gezelius E. Cross-laminated timber flooring and concrete slab flooring: A comparative study of structural design, economic and environmental consequences. J Build Eng 2019;100881.
[10] Zingg S, Habert G, Lämmlein T, Lura P, Denarié E, Hajiesmaeili A. Environmental assessment of radical innovation in concrete structures. Expand Boundaries Syst Think Built Environ 2016.
[11] Fauzi RT, Lavoie P, Sorelli L, Heidari MD, Amor B. Exploring the current challenges and opportunities of life cycle sustainability assessment. Sustainability 2019;11(3):636.
[12] Bouhaya L, Le Roy R, Feraille-Fresnet A. Simplified environmental study on innovative bridge structure. Environ Sci Technol 2009;43(6):2066–71.
[13] Bathon L, Graf M. A continuous wood-concrete-composite system. In: Proc, World Conference of Timber Engineering, Whistler, BC; 2000.
[14] Lehan AR. Development of a Slab-on-Girder Wood-Concrete Composite Highway Bridge. University of Toronto (Canada); 2012.
[15] Frangi A, Fontana M. Elasto-plastic model for timber-concrete composite beams with ductile connection. Struct Eng Int 2003;13(1):47–57.
[16] Pluess Y, Zwicky D. Plastic Design of Timber Concrete Composite Girders. London: IABSE/IASS; 2011.
[17] Dias AM, Jorge LF. The effect of ductile connectors on the behaviour of timber–concrete composite beams. Eng Struct 2011;33(11):3033–42.
[18] Zhang C. Analysis of the Timber-Concrete Composite Systems with. Ductile Connection 2013.
[19] Zhang C, Gauvreau P. Timber-concrete composite systems with ductile connections. J Struct Eng 2014;141(7):04014179.
[20] Clouston P, Bathon LA, Schreyer A. Shear and bending performance of a novel wood–concrete composite system. J Struct Eng 2005;131(9):1404–12.
[21] Auclair-Cuerrier S, Sorelli L, Salenikovich A. A new composite connector for timber-concrete composite structures. Constr Build Mater 2016;112:84–92.
[22] Selçukoglu E, Zwicky D. Towards the plastic design of glulam concrete composite structures. In: In: IABSE Symposium Report. International Association for Bridge and Structural Engineering; 2009. p. 20–9.
[23] Lamothe S, Sorelli L, Blanchet P, Galimard P. Engineering ductile notch connections for composite floors made of laminated timber and high or ultra-high performance fiber reinforced concrete. Eng Struct 2020;211:110415.
[24] Jiang Y, Crocetti R. CLT-concrete composite floors with notched shear connectors. Constr Build Mater 2019;195:127–39.
[25] Boccadoro L, Zweidler S, Steiger R, Frangi A. Calculation model to assess the structural behavior of LVL-concrete composite members with ductile notched connection. Eng Struct 2017;153:106–17.
[26] Mai KQ, Park A, Nguyen KT, Lee K. Full-scale static and dynamic experiments of hybrid CLT–concrete composite floor. Constr Build Mater 2018;170:55–65.
[27] Pham HS. Optimisation et comportement en fatigue de la connexion bois-BFUP pour de nouveaux ponts mixtes. École nationale des ponts et chaussées (France). 2007.
[28] Kong K, Ferrier E, Michel L. Creep Behaviour of Heterogeneous Timber-UHPFRC Beams Assembled by Bonding: Experimental and Analytical Investigation. World Acad Sci Eng Technol Int J Civ Environ Struct Constr Archit Eng 2015;9(9):1197–204.
[29] Ferrara L, Cremonesi M, Faifer M, Toscani S, Sorelli L, Baril M-A, et al. Structural elements made with highly flowable UHPFRC: Correlating computational fluid dynamics (CFD) predictions and non-destructive survey of fiber dispersion with failure modes. Eng Struct 2017;133:151–71.
[30] Naud N, Sorelli L, Salenikovich A, Cuerrier-Auclair S. Fostering UHPFRC-Glulam Laminated Timber Composite Structure for Multi-storey Buildings. Elsevier. Eng Struct 2019. accepted for publication in /02/2019.
[31] Ferrier E, Labossiere P, Neale KW. Mechanical behavior of an innovative hybrid beam made of glulam and ultrahigh-performance concrete reinforced with FRP or steel. J Compos Constr 2009;14(2):217–23.
[32] Graybeal B, Crane CK, Perry V, Corvez D, Ahlborn TM. Advancing Ultra-High-Performance Concrete. Concr Int 2019;41(4):41–5.
[33] Pham HS. Optimisation and fatigue behaviour of interface wood-UHPFRC for new composite bridges. Ecole des Ponts ParisTech 2007.
[34] Auclair-Cuerrier S, Sorelli L, Salenikovich A. Simplified nonlinear model for timber-concrete composite beams. Int J Mech Sci 2016;117:30–42.
[35] Gendron B, Salenikovich A, Sorelli L. Timber Concrete Composite Beams with Ductile Connection. In: World Conference on Timber Engineering. 2016.
[36] En B. Eurocode 5: Design of timber structures—General—Common rules and rules for buildings. NA to BS EN 1995;1–1:2004.
[37] Möhler K. On the load carrying behavior of beams and columns of compound sections with flexible connections. Technical Univ of Karlsruhe Germany 1956.
[38] Van der Linden M. Timber-concrete composite beams. Heron 1999.
[39] Newmark NM. Test and analysis of composite beams with incomplete interaction. Proc Soc Exp Stress Anal 1951;9(1):75–92.
[40] Fragiacomo M. A finite element model for long-term analysis of timber-concrete composite beams. Struct Eng Mech 2005;20(2):173–89.
[41] Khorsandnia N, Valipour HR, Crews K. Nonlinear finite element analysis of timber beams and joints using the layered approach and hypoelastic constitutive law. Eng Struct 2013;46:606–14.
[42] Graybeal BA. Material property characterization of ultra-high performance concrete; 2006.

[43] Canadian Highway Bridge Design Code. CSA S6 Annex 8.1 Fibre Reinforced Concrete. In: CSA S6 standard; 2019.
[44] Naud N. Développement des structures composites bois-béton avec emphase sur le comportement de la connexion 2018;113.
[45] NBCC N. National building code of Canada. Natl Res Counc Can NRCC Ott Can. 2005.
[46] Cuerrier-Auclair S. Technical Design Guide For Timber-Concrtee Composite Floors in Canada. Quebec City, Canada: FPInnovations; 2019. p. 91.
[47] FRAGIACOMO M, CECCOTTI A. A Simplified Approach for Long-Term Evaluation of Timber-Concrete Composite Beams. 2014 May;7.
[48] AFGC publication. Bétons fibrée à ultra-hautes performances- Recommandations; 2013.
[49] Association CS. Design of concrete structures. Mississauga, Ont.: Canadian Standards Association; 2004.
[50] ISO 18324. ISO: Timber Structures - Test Methods - Floor Vibration Performance. ISO 18324; 2016.
[51] Association CS. CSA O86–14: Engineering Design in Wood. Can Stand Assoc 2014; 178:196.
[52] Nordic. Documents techniques, Nordic X-Lam; 2017.
[53] Gagnon S, Karacabeyli E. Canadian cross laminated timber (CLT) handbook. FPInnovations Vanc Can 2019.
[54] Bajzecerová V. Bending stiffness of clt-concrete composite members-comparison of simplified calculation methods. Procedia Eng 2017;190:15–20.
[55] Standard A. Standard Test Method for Compressive Strength of Cylindrical Concrete Specimens; 2018.
[56] Standard A. Standard Test Method for Static Modulus of Elasticity and Poisson's Ratio of Concrete in Compression; 2014.
[57] King Materials. Documents techniques, King Materials; 2017.
[58] CEN E. 26891–Timber structures. Joints made with mechanical fasteners general principles for the determination of strength and deformation characteristics. ISO EN. 1991;26891.
[59] Gendron B. Ponts composites bois-béton collaborant en portée simple: théorie, essais et conception. Université Laval 2016.
[60] Mushina J, Ghafar NA, Yeoh D, Mushina W, Boon KH. Vibration Behaviour of Natural Timber and Timber Concrete Composite Deck System. In: In: IOP Conference Series: Materials Science and Engineering. IOP Publishing; 2020. p. 012023.
[61] Lamothe S, Luca, Sorelli. Development of a Rigid-Ductile Notch Connector for Timber Composite Structures with Cross Laminated and Glued Laminated Timber; 2018.
[62] Auclair SC, Sorelli L, Salenikovich A. Simplified nonlinear model for timber-concrete composite beams. Int J Mech Sci 2016 Oct;117:30–42.